RESEARCH REPORT

Contract nr.:	194/2017 (PN-III-P4-ID-PCE-2016-0649)
Project:	Parallel theoretical study of the two components of the prompt fission neutrons: dynamically released at scission (SN) and evaporated from fully accelerated fragments (EVN)
Project director:	Dr. Nicolae Carjan
Phase nr. 2/2018:	The calculus of the time dependence of the decay rate. The dependence of the energy spectrum and of the angular distribution of the scission neutrons on the quantum number Ω.

1 Phase objective

This calculation will reveal the dynamics of the emission process. It will be established how long it takes before 10%, 50% and 90% of neutrons leave the fissioning nucleus. The evaluation of the relative contribution of each set of neutron eigenstates (Ω) to the angular distribution will allow to determine the angular domains that are populated by neutrons with different Ω values. From the energy spectra over all Ω value one obtains the whole kinetic energy spectrum, which is compared with the measured spectrum of all prompt fission neutrons.

2 Activities

The study of the competition between the two components of the prompt fission neutrons in the region where the evaporated (EVN) and the scission neutrons (SN) overlap - Part I.

3 Phase report

3.1 Introduction

The purpose of the project is to provide elements for answering the important question of the nature and relative abundance of the two components of prompt fission neu-

trons (PFN): released at scission (SN) and evaporated from fully accelerated fragments (EVN).

We have used a dynamical scission model to estimate the main properties of the scission neutrons (SN), based on the solution of the time-dependent Schrödinger equation [1], [2]. When the calculated data have been compared with measurements of PFN during 235U(n_{th},f) the experimental trends are well reproduced. Based on this evidence, one cannot decide anymore which is the main source of PFN. It is therefore necessary to extend the application of our model to other observables and other fissioning systems to see how far this agreement holds. Also, the same quantities will be calculated with both models (scission and evaporation) to decide which is more realistic.

In the previous phase we have studied the shape of the energy spectrum of neutrons emitted during scission through the Fourier transform of single particle wave functions in spherical and deformed nuclei.

In the present phase we determine the time dependent decay rate for the neutrons leaving a sphere around the nucleus. This provides additional informations about the evolution of the emission process. Thus, it will be evaluated the time necessary for different amount of neutrons to be released from the fissioning nucleus and it will be shown the character of the SN emission (exponential or oscillatory). The dependence of the decay rate on the quantum number Ω and on the radius of the sphere around the nucleus is also studied. The scission-neutron angular distribution and the energy spectrum are calculated for different time intervals and for several Ω values as well. Relevant features of the two types of neutrons (of scission and evaporated) are discussed.

3.2 Formalism

To study the neutrons released during scission we consider single particle wave functions in cylindrical coordinates. The neutron wave packets are propagated through the bi-dimensional time dependent Schrödinger equation (TDSE) with time dependent potential (TDP):

$$i\hbar\frac{\partial\Psi(\rho,z,t)}{\partial t}=\mathcal{H}(\rho,z,t)\Psi(\rho,z,t), \tag{1}$$

$$\mathcal{H}\Psi=\begin{bmatrix} O_1-CS_c & -CS_a \\ -CS_b & O_2-CS_d \end{bmatrix}\begin{bmatrix} f_1 \\ f_2 \end{bmatrix},\quad O_{1,2}=-\frac{\hbar^2}{2\mu}(\Delta-\frac{\Lambda_{1,2}^2}{\rho^2})+V(\rho,z,t). \tag{2}$$

Δ is the Laplacean, V is the potential, C is a constant and the operators $S_a,\ldots,S_d$ represent the spin-orbit coupling. We use a realistic mean field potential of Woods-Saxon type adapted to nuclear shapes described by generalized Cassini ovals [3]. The wave functions have two components corresponding to spin "up" and spin "down". For a given projection Ω of the total angular momentum on the symmetry axis they assume the form:

$$|\Psi\rangle=f_1(\rho,z)\mathrm{e}^{\mathrm{i}\Lambda_1\theta}|\uparrow\rangle+f_2(\rho,z)\mathrm{e}^{\mathrm{i}\Lambda_2\theta}|\downarrow\rangle,\quad \Lambda_1=\Omega-\frac{1}{2},\ \Lambda_2=\Omega+\frac{1}{2}. \tag{3}$$

Due to the axial symmetry, only the coordinates ρ and z remain.

3.3 Dynamical Scission Model

According to the Dynamical Scission Model [1], [2], we separate the calculation in two stages:

1)The scission process itself, i.e., the neck rupture and its absorption by the fragments. The nuclear configuration just before scission is represented by the deformation set $\{\alpha^i\}$, while immediately after scission it is represented by the set $\{\alpha^f\}$.

2)The detachment from the fragments of the fraction of the neutrons that are left unbound at the end of the previous stage. Since, at this stage, their motion is much faster than that of the just separated fragments we maintain the fragments at the configuration $\{\alpha^f\}$.

In the 1st stage we follow the time evolution of the wave functions corresponding to each neutron state that is occupied at $\{\alpha^i\}$. At each time step the nuclear shape and the potential is changing as the deformation parameter set varies uniformly from $\{\alpha^i\}$ to $\{\alpha^f\}$. The initial wavefunctions (at $t = 0$) are taken as eigensolutions of the eigenvalue problem: $\mathcal{H}\Psi = E\Psi$. To solve it, we limit our domain to a finite grid with the mesh points of the coordinates (ρ_j, z_k). At each point the partial derivatives in $\mathcal{H}$ are approximated by finite difference formulas [4]. The eigenvalue problem is transformed into an algebraic eigenvalue problem, which is solved by an appropiate method (Arnoldi) [5]. The propagation in time is performed by a scheme of Crank-Nicolson type [6].

In the 2nd stage we follow the evolution of these wave packets (that describe the unbound neutrons) in time (by TDSE with the potential fixed for the set $\{\alpha^f\}$).

The solutions of TDSE are used to calculate quantities like:

1. **The probability amplitude** that a neutron occupying the state $|\Psi^i\rangle$ before scission populates an eigenstate $|\Psi^f\rangle$ after a time interval T:

$$a_{if} = \langle \Psi^i(T)|\Psi^f\rangle = 2\pi \int\int (f_1^i(T) f_1^f + f_2^i(T) f_2^f)\rho d\rho dz. \tag{4}$$

2. **The emitted part** of the wave packet:

$$|\Psi^i_{em}\rangle = |\Psi^i(T)\rangle - \sum_{bound} a_{if}|\Psi^f\rangle. \tag{5}$$

   It leaves the fissioning nucleus and asymptotically describes the emitted scission neutron. The Fourier transforms of the unbound-neutron wave packets give, at each time, the momentum distributions and therefore also the kinetic energy distributions. Asymptotically, the sum over all neutrons, weighted with their occupation probabilities v_i^2, leads to the scission neutron spectrum.

3. **The current density**, a vector defined as

$$\bar{J}^i_{em}(\rho, z, T) = \frac{\mathbf{i}}{\hbar}\frac{\hbar^2}{2\mu}(Y\nabla Y^* - Y^*\nabla f) = J^i_\rho \bar{e}_\rho + J^i_z \bar{e}_z, \tag{6}$$

with $Y = |\Psi^i_{em}\rangle$. The vector $\bar{J}_{em}$ for all states has the components:

$$J_\rho(\rho, z, T) = 2 \times \sum_i v_i^2 J_\rho^i, \quad J_z(\rho, z, T) = 2 \times \sum_i v_i^2 J_z^i.$$

4. **The number of neutrons** that leave a sphere of radius R (around the fissioning nucleus) in a solid angle $d\Omega$ and in a time interval dt is:

$$d\nu_{sc}^{em} = \bar{J}_{em}(R, \theta, t)\bar{n}(R, \theta, t)R^2 dt d\Omega. \tag{7}$$

5. **The angular distribution** given by the integral with respect to t of the above quantity. The upper limit should in principle be ∞. In practice we can reach only a finite value T_{max}. By a further integration with respect to θ ($d\Omega = \sin\theta d\theta$) one obtains the total number of emitted neutrons (ν_{sc}^{em}) at T_{max}.

6. **The total escape probability** given by the fraction of the wave function located beyond a shere of radius R around the nucleus at the time t:

$$P_{tun}(t) = 2\pi \int_{D_{ext}} |\Psi(\rho, z, t)|^2 \rho d\rho dz. \tag{8}$$

7. **The total decay rate** related to the total escape probability by

$$\lambda(t) = \frac{1}{N_{tot} - P_{tun}} \frac{dP_{tun}(t)}{dt} \tag{9}$$

where N_{tot} is the total norm given by

$$N_{tot}(t) = 2\pi \int_D |\Psi(\rho, z, t)|^2 \rho d\rho dz. \tag{10}$$

The infinite total domain D is limited in calculations to a finite one by the numerical boundaries. In practice, $N_{tot} - P_{tun}$ is replaced by

$$N_{int}(t) = 2\pi \int_{D_{int}} |\Psi(\rho, z, t)|^2 \rho d\rho dz \tag{11}$$

which is more convenient for calculations. The domain D_{int} is delimited by the semicircle of radius R, while the domain D_{ext} is the complementary of D_{int} with respect to D.

3.3.1 Calculus of $\frac{dP_{tun}(t)}{dt}$

The calculation of dP_{tun}/dt requires a particular attention. One way would be to evaluate the two-dimensional integral on the domain D_{ext} and then numerically obtain the derivative with respect to time. But, apart the difficulty to calculate an integral in two dimensions, the entire wavefunction outside the numerical domain will be neglected. This introduces a crude approximation which can spoil the value of λ. A simpler and more accurate method to calculate dP_{tun}/dt is by the flux.

We make use of **the continuity equation** (see [7]):

$$\frac{\partial p}{\partial t} + \nabla J = 0 \tag{12}$$

where $p(r,t) = |f(r,t)|^2$ is **the probability density** (r being the spatial coordinate vector and f being the solution of TDSE), while $J(r,t)$ is the **the current density**.

$$\nabla J(r,t) = divJ(r,t) = -\frac{i}{\hbar}\frac{\hbar^2}{2\mu}(f^*\Delta f - f\Delta f^*) \tag{13}$$

represents **the flux**. The expression of ∇J in cylindrical coordinates is (see [7]):

$$\nabla J = -\frac{i}{\hbar}\frac{\hbar^2}{2\mu}\left\{\frac{1}{\rho}\frac{\partial}{\partial\rho}\left[\rho\left(f^*\frac{\partial f}{\partial\rho} - f\frac{\partial f^*}{\partial\rho}\right)\right] + \frac{\partial}{\partial z}\left(f^*\frac{\partial f}{\partial z} - f\frac{\partial f^*}{\partial z}\right)\right\}. \tag{14}$$

According to the continuity equation, we have:

$$\frac{dP_{tun}(t)}{dt} = \frac{d}{dt}\left(2\pi\int_{D_{ext}}|f(\rho,z,t)|^2\rho d\rho dz\right) = -2\pi\int_{D_{ext}}\nabla J\rho d\rho dz =$$

$$= 2\pi\frac{i}{\hbar}\frac{\hbar^2}{2\mu}\left\{\int_{D_{ext}}\frac{\partial}{\partial\rho}\left[\rho\left(f^*\frac{\partial f}{\partial\rho} - f\frac{\partial f^*}{\partial\rho}\right)\right]d\rho dz + \int_{D_{ext}}\frac{\partial}{\partial z}\left[\rho\left(f^*\frac{\partial f}{\partial z} - f\frac{\partial f^*}{\partial z}\right)\right]d\rho dz\right\}.$$

Let us note

$$P(\rho,z) = \rho\left(f^*\frac{\partial f}{\partial\rho} - f\frac{\partial f^*}{\partial\rho}\right), Q(\rho,z) = \rho\left(f^*\frac{\partial f}{\partial z} - f\frac{\partial f^*}{\partial z}\right).$$

Thus one can write

$$\frac{dP_{tun}(t)}{dt} = 2\pi\frac{i}{\hbar}\frac{\hbar^2}{2\mu}\left(\int_{D_{ext}}\frac{\partial P}{\partial\rho}d\rho dz + \int_{D_{ext}}\frac{\partial Q}{\partial z}d\rho dz\right) = 2\pi\frac{i}{\hbar}\frac{\hbar^2}{2\mu}(I_1 + I_2). \tag{15}$$

We consider now the domain D_{ext}. It is delimited by the semicircle of radius R (i.e. the radius of the considered sphere) and the limits of the numerical domain. The circular curve is expressed either as a function of $z:\ \rho = u(z)$ or as a function of $\rho:\ z = v(\rho)$ (see Fig.1). The double integrals are transformed into curvilinear integrals, according to some mathematical rules from the integral calculus (the Riemann-Green formula). Using the notations of figure 1 we can write:

$$I_1 = \int_{-z_{max}}^{-z_b} dz\int_{\rho_1}^{\rho_{max}}\frac{\partial P}{\partial\rho}d\rho + \int_{-z_b}^{z_b} dz\int_{\rho=u(z)}^{\rho_{max}}\frac{\partial P}{\partial\rho}d\rho + \int_{z_b}^{z_{max}} dz\int_{\rho_1}^{\rho_{max}}\frac{\partial P}{\partial\rho}d\rho$$

$$= \int_{-z_{max}}^{-z_b}\left[P(\rho_{max},z) - P(\rho_1,z)\right]dz + \int_{-z_b}^{z_b}\left[P(\rho_{max},z) - P(u(z),z)\right]dz +$$

$$+ \int_{z_b}^{z_{max}}\left[P(\rho_{max},z) - P(\rho_1,z)\right]dz.$$

$-z_b$ and z_b are the points where the circular curve crosses the axis $\rho = \rho_1$. The considered case has a symmetry with respect to $z = 0$, so that we can limit ourselves

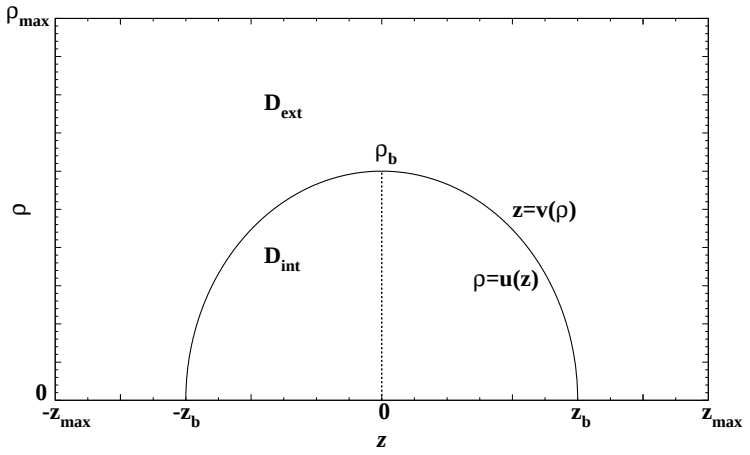

Figure 1: A representation of the regions implied in the calculation of the decay rate.

to a half of domain. When we don't have such a symmetry, the above formula can be used with an appropriate adaptation.

Thus, for the configuration in fig.1 we have

$$\frac{1}{2}I_1 = \int_0^{z_b} \left[P(\rho_{max}, z) - P(u(z), z)\right] dz + \int_{z_b}^{z_{max}} \left[P(\rho_{max}, z) - P(\rho_1, z)\right] dz.$$

Similarly,

$$\frac{1}{2}I_2 = \int_{\rho_1}^{\rho_b} d\rho \int_{z=v(\rho)}^{z_{max}} \frac{\partial Q}{\partial z} dz + \int_{\rho_b}^{\rho_{max}} d\rho \int_0^{z_{max}} \frac{\partial Q}{\partial z} dz =$$

$$= \int_{\rho_1}^{\rho_b} \left[Q(\rho, z_{max}) - Q(\rho, v(\rho))\right] d\rho + \int_{\rho_b}^{\rho_{max}} \left[Q(\rho, z_{max}) - Q(\rho, 0)\right] d\rho.$$

ρ_b is the point where the circular curve meets the axis $z = 0$. (In fact, $\rho_b = R$). Now, the terms containing the values ρ_{max} and z_{max}, belonging to the boundaries, are considered zero, since theoretically ρ_{max}, z_{max} tend to ∞ and there the wavefunction should be zero. It results :

$$\frac{1}{2}I_1 = -\int_0^{z_b} P(u(z), z) dz - \int_{z_b}^{z_{max}} P(\rho_1, z) dz \tag{16}$$

and

$$\frac{1}{2}I_2 = -\int_{\rho_1}^{\rho_b} Q(\rho, v(\rho)) d\rho - \int_{\rho_b}^{\rho_{max}} Q(\rho, 0) d\rho. \tag{17}$$

Thus, the only values which we are obliged to neglect in the numerical calculation are $f(\rho_1, z), z > z_{max}$ and $f(\rho, 0), \rho > \rho_{max}$, which are normally small.

Using the equations (16), (17) one can obtain I_1, I_2 and then $dP_{tun}(t)/dt$ from equation (15) (note that its value is strictly real). Of course, in practice the circular curve, the first derivatives with respect to ρ, z and the uni-dimensional integrals are evaluated approximately, since the wavefunction values are known only in the grid points.

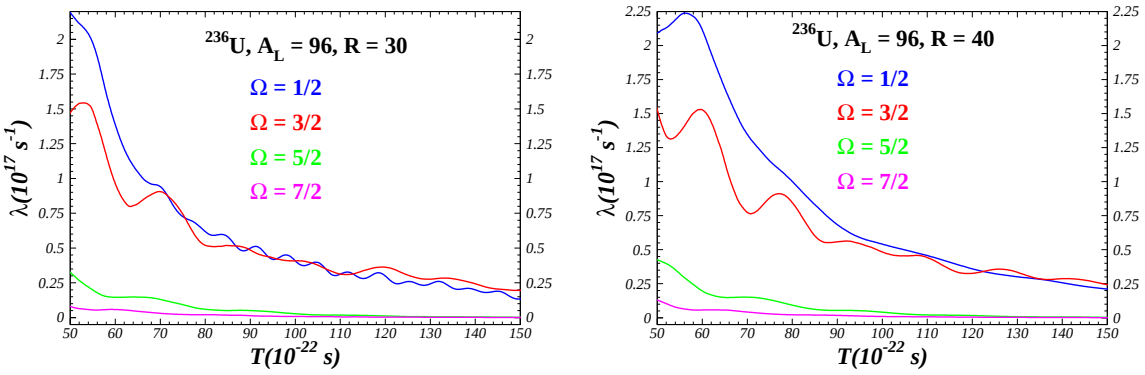

Figure 2: Scission-neutron decay rates as functions of time calculated on spheres of radius R=30 fm (left) and R=40 fm (right) with sets of neutron wave functions characterized by a given quantum number Ω.

3.4 Results

We have investigated the reaction $^{235}U(n_{th}, f)$ with the light fragment mass $A_L = 96$ (which is the most probable experimental mass asymmetry). Two parameters of the Cassini representation have been considered: α (elongation) and α_1 (mass asymmetry). We have chosen: $\alpha = 0.985$ (before scission) and $\alpha = 1.001$ (after scission). The parameter α_1 results from the condition of fixed ratio of the fragment volumes that corresponds to A_L=96.

Fig. 2 shows the time-dependent decay rate for 2 values of the radius R (30 and 40 fm) of the sphere that separates the external from the internal domain. The results are presented separately for sets of neutron wave functions characterized by a given value of the quantum number Ω. One can see that $\lambda(t)$ has an oscillatory behaviour immediately after the neck rupture. With increasing time the amplitude of these oscillations diminishes and asymptotically reaches an almost constant value indicative of an exponential decay. This feature is more visible at high Ω values (5/2 and 7/2) where there is a centrifugal barrier to be tunneled. Fig. 3 shows the comparison of the time dependent decay rate for the 2 values of the radius R. One sees that although the neutron flux needs longer time to reach the larger sphere, asymptotically they tend to the same value. This result constitutes a validity test of our calculations.

Table 1 shows how long it takes for scission neutrons with different Ω values to be emitted, i.e., to find themselves outside the sphere with R=40 fm. The values in this table were obtained from Fig. 4 where the survival probability (eq. (11)) is plotted as a function of time. This probability tends to a constant value that is non-zero since only a small fraction of the neutrons are emitted during scission. One can see that half of the unbound neutrons are emitted at 3×10^{-21} sec (if Ω=1/2) and at 1.5×10^{-21} (if Ω=9/2). This is the order of magnitude of the 'half-life' of the emission of neutrons at scission.

Fig. 5 shows the angular distribution with respect to the fission axes of scission neutrons with projection of the angular momentum Ω=1/2 at 4 consecutives times after the neck

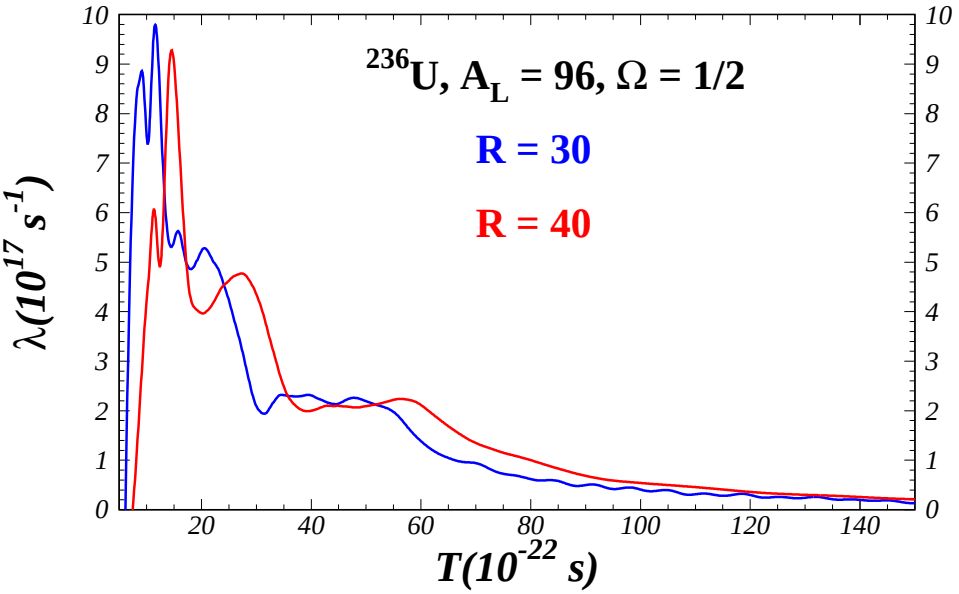

Figure 3: Comparison between the time dependent decay rates calculated on spheres with different radii R.

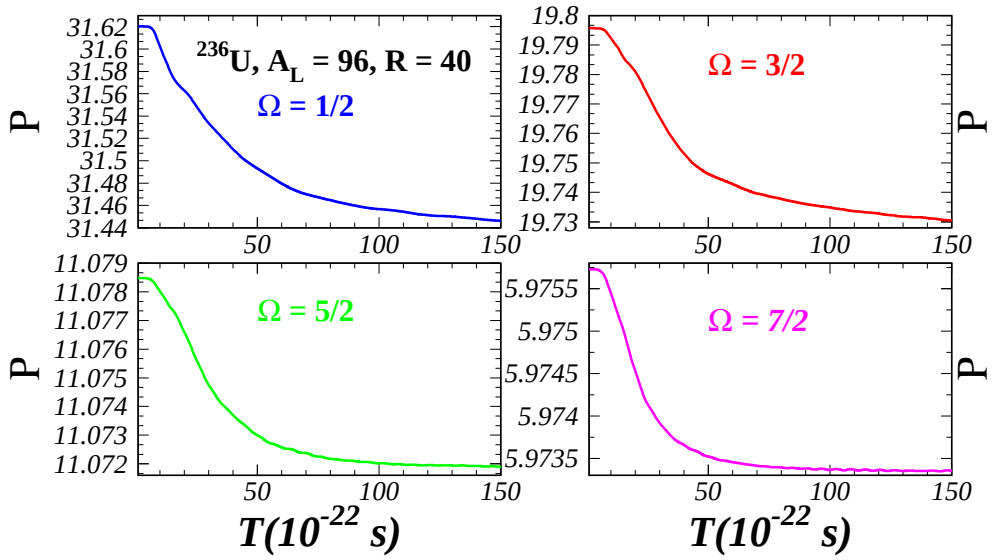

Figure 4: Neutron survival probabilities as a function of time calculated with eq. (11) for different values of Ω.

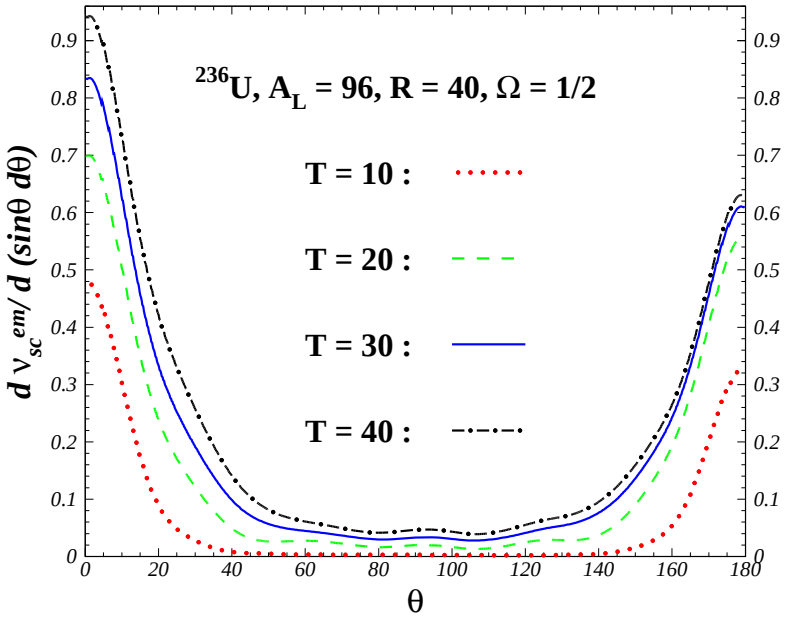

Figure 5: Scission-neutron angular distribution for Ω=1/2 at different times after scission (T is in 10^{-22} s).

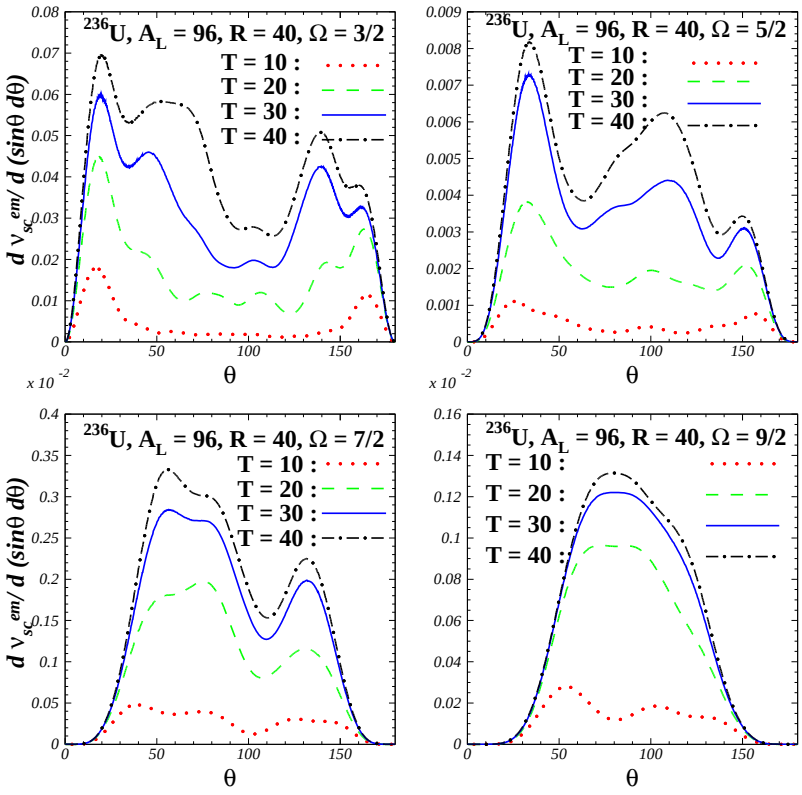

Figure 6: The same as in Fig. 5 but for larger values of Ω

Table 1: Time necessary for 10%,50% and 90% of the scission neutrons to leave the sphere with R=40 fm as a function of Ω.

Ω	$T(10\%)$	$T(50\%)$	$T(90\%)$
1/2	9.9×10^{-22}s	30.2×10^{-22}s	82.2×10^{-22}s
3/2	12.7×10^{-22}s	31.7×10^{-22}s	84.3×10^{-22}s
5/2	11.6×10^{-22}s	27.4×10^{-22}s	60.3×10^{-22}s
7/2	9.4×10^{-22}s	19.9×10^{-22}s	45.1×10^{-22}s
9/2	8.7×10^{-22}s	15.8×10^{-22}s	34.7×10^{-22}s

rupture. The emission takes place mainly along the fission axes with a preference for the direction of the light fragment as in experiment. So the most probable angles are 0° and 180°. Fig. 6 shows the drastic change of the angular distribution due to the value of Ω. At Ω=3/2 already, there is no emission at 0° and 180° and this trend accentuates with increasing Ω so that at Ω=9/2 the most probable angle is perpendicular to the fission axes as in the case of charged particles (mainly alpha particles) which accompany the fission process. In this respect the scission neutrons are totaly different from the evaporated neutrons and this difference could be used to distinguish between the two components. The evaporated neutrons are emitted isotropically in the fragments frame. The anisotropy of their angular distribution in the laboratory system is simply due to the kinematics of the post scission separation of the fragments. It has therefore nothing to do with the intrinsic properties of the neutrons (such as Ω).

The upper five frames of Fig.7 show as histograms kinetic energy spectra for Ω=1/2 until Ω=9/2. The average kinetic energy increases with increasing Ω due to the centrifugal term. In the 6th frame, the total spectrum (summed over the five Ω values) is shown. For comparison, we added recent data [8] obtained for the same constraint on mass asymmetry ($A_L = 96$). One notices that both the data and the calculation are not smooth. The calculated distribution is not smooth since it consists of a finite weighted sum of individual contributions with different mean values and widths. Two typical evaporation spectra [9], $E\exp(-E/Temp)$, for nuclear temperatures $Temp = 1.0$ and 0.9 MeV are also ploted. These evaporation spectra follow quite well the general trend of the recent data except at very low and very high energies. In the lowest frame of Fig.7 the same comparison is shown in lin-log scale to unveil hidden differences at $E_{kin} > 5$ MeV. One can see that, in contrast to the EVN, the SN can reproduce the high energy tail of the PFN spectrum.

3.5 Summary and Conclusions

The decay rate λ of the scission-neutron emission is time dependent. At short times after scission λ(t) oscillates: we are dealing with a pulsed emission. At large times

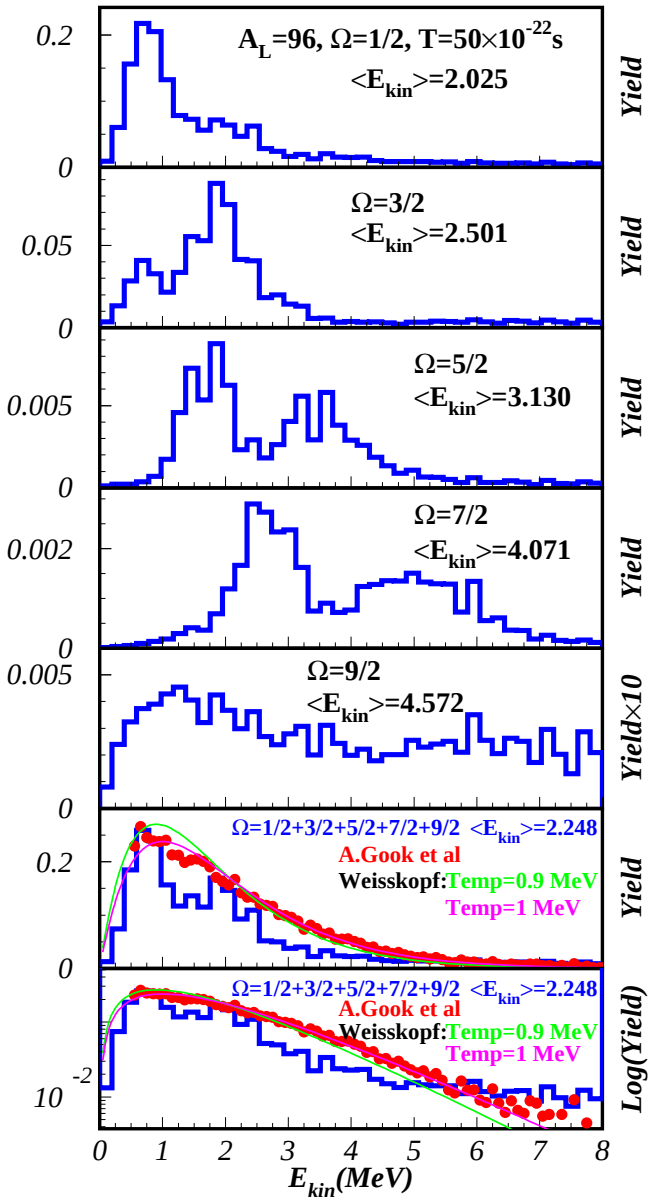

Figure 7: Kinetic energy distributions at $T = 50 \times 10^{-22}$ sec for sub-states defined by the quantum number Ω. In the two lowest frames the distribution calculated with all neutron states is presented together with recent experimental results from the reaction $^{235}U(n_{th}, f)$. Two typical evaporation spectra are also plotted for comparison.

the oscillations are damped and λ tends to an almost constant value: we are dealing with and exponential decay. The transition between these two behaviours depends on the quantum number Ω. From the time dependence of the survival probability $N_{int}(t)$ we deduced the 'half-life' of the scission-neutron emission: $\approx 2.5 \times 10^{-21}$ sec. So the emission starts during the scission process and covers the first part of the fragments acceleration phase.

The angular distribution of the scission neutrons with respect to the fission axes (hence in the laboratory system) was calculated for sets of neutron wavefunctions defined by a given Ω value (1/2, 3/2, 5/2, 7/2 and 9/2). A strong dependence on Ω was found. Namely, wave functions with different Ω have different most probable emission angles: from emission along the fission axes (1/2) to emission perpendicular to the fission axes (9/2). This result leads to a new interpretation of the measured angular distribution of the PFN, completely different from the one provided by the EVN hypotheses. It may open a possibility to separate the two components of the PFN.

Concerning the energy spectrum we note that the SN spectrum presents structures, in qualitative agreement with the measured spectrum. However the experimental data do not oscillate as much as the calculations. One reason is that the data are affected by a finite energy resolution. If we convolute the theoretical spectrum with a Gaussian resolution function, the amplitude of its oscillations will decrease. The evaporation hypothesis is unable to account for high energy PFN as was also pointed out in Ref.[10].

References

[1] M. Rizea, N. Carjan, Nuc. Phys. A **909**, 50–68 (2013)

[2] N. Carjan, M. Rizea, Phys. Lett. B **747**, 178–181 (2015)

[3] V.V. Pashkevich, Nucl. Phys. A **169**, 275–293 (1971)

[4] M. Rizea, V. Ledoux, M. Van Daele, G. Vanden Berghe, N. Carjan, Comp. Phys. Commun. **179**, 466–478 (2008)

[5] R. B. Lehoucq , D. C. Sorensen, C. Yang, *ARPACK Users Guide* (Philadelphia, SIAM, ISBN 978-0-89871-407-4, 1998)

[6] M. Rizea, N. Carjan, Proc. Rom. Acad. A **16**, 176–183 (2015)

[7] C.Cohen-Tannoudji, B.Diu, F.Laloë, *Mécanique Quantique*, Hermann, Paris (1973)

[8] A. Göök, F.-J. Hambsch, W. Geertz, M. Vidali, private communication

[9] J. M. Blatt, V. F. Weisskopf, *Theoretical Nuclear Physics* (John Wiley, New York, 1958) 368

[10] N. Kornilov, *Fission Neutrons: Experiments, Evaluation, Modeling and Open Problems*, Springer, Switzerland (2015).